The data supporting this article have been included as part of the Supplementary Information.

Chemical and physical pressure meet: deciphering the polymorphism and morphology of α- and δ-KY_3F_{10} induced by Eu^{3+} doping

Samantha Custódio Silva Lemos[1]*, Pablo Serna-Gallén[2], Lourdes Gracia[1,3]*, Eduardo O. Gomes[1], Héctor Beltrán-Mir[2], Eloísa Cordoncillo[2], Juan Andrés[1]*

[1]*Departamento de Química Física y Analítica, Universitat Jaume I, Av. Vicent Sos Baynat s/n 12071, Castelló de la Plana, Spain*

[2]*Departamento de Química Inorgánica y Orgánica, Universitat Jaume I, Av. Vicent Sos Baynat s/n 12071, Castelló de la Plana, Spain*

[3]*Department of Physical Chemistry, University of Valencia (UV), 46100 Burjassot, Spain*

*Corresponding Authors

Supplementary Information

1. Experimental section

1.1. Materials

The reagents used for the synthesis of the powders were yttrium(III) nitrate hexahydrate [$Y(NO_3)_3 \cdot 6H_2O$ 99.8%], europium(III) nitrate hexahydrate [$Eu(NO_3)_3 \cdot 6H_2O$ 99.9%], and potassium fluoride [KF 99.5%]. All reagents were purchased from Sigma-Aldrich, except europium(III) nitrate hexahydrate (Strem Chemicals), and used without further purification.

1.2. Synthesis of the powders

Calculations were performed to obtain approximately 0.25 g of KLn_3F_{10} (Ln = Y, Eu).

Different nominal compositions were formulated to study the evolution of the crystal phase transition and the morphology of the particles. For that purpose, the nominal percentages of Eu^{3+} used were: 10, 15, 20, 30, 40, 50, and 100 mol% with respect to the total amount of Ln. Samples were denoted as "S-*n*", where *n* indicates the percentage of Eu^{3+}.

All the samples were prepared following a coprecipitation method at room temperature. First, 1.5 mmol of $Ln(NO_3)_3 \cdot 6H_2O$ were dissolved in 10 mL of water. Then, another solution containing 3 mmol of KF and 3 mmol of HF was prepared. The latter solution was added dropwise to the previously prepared Ln^{3+} solution yielding the formation of a white precipitate, which was kept under vigorous stirring for 1 hour. After that time, it was collected by centrifuging the mixture and washing it twice with water. Finally, the precipitate was dried under an infrared lamp to obtain the desired powder.

1.3. Characterization

All the characterization of the materials was performed at room temperature. Powder X-ray diffraction (XRD) was carried out using a Bruker-AX D8-Advance X-ray diffractometer with Cu$K_{\alpha 1}$ radiation from 2θ = 15 to 90º at a scan speed of 1.8º/min. The FT-IR spectra of the solids were recorded using a JASCO FT/IR-6800 spectrometer in transmission mode. The microstructure of samples was observed using a GeminiSEM500 (ZEISS) high-resolution scanning electron microscope (HRSEM) operating with an acceleration voltage of 3.5 kV, a measuring time of 20 s, and a working distance of 5.1 mm. For microstructural characterization, the powders were deposited on carbon double-sided stickers (previously adhered to the surface of aluminum stubs) and were sputtered with platinum.

Table S1 shows the Inductively Coupled Plasma Mass Spectrometry (ICP-MS) values for Eu composition of the samples.

Table S1. ICP-MS

Sample	Eu mol%
S-10	9.9 ± 0.2
S-15	16.3 ± 0.2
S-20	20.1 ± 0.2
S-30	29.9 ± 0.2
S-40	45.4 ± 0.4
S-50	50.9 ± 0.4
S-100	99.72 ± 0.01

Table S2. Experimental (S10 and S20 samples) and calculated IR frequencies of α and δ-KY_3F_{10} polymorphs at 8.3% and 16.7% of Eu^{3+} doping. In parenthesis the number of modes.

	IR frequencies (cm^{-1})			
α-KY_3F_{10}	8.3% Eu^{3+}	16.7% Eu^{3+}	S20	Assignation
243.5	236.3-244.1 (4)	232.00-247.3 (5)	231	Bending Y-F-K
315.4	305.4-313.4 (4)	304.5-317.8 (5)	276	Bending F-Y-K
360.5	357.11-359.6 (3)	354.8-368.2 (5)	364	Bending F-Y-F
508.1	503.9-514.8 (6)	506.2-511.9 (3)	500	Stretching F-Y

	IR frequencies (cm^{-1})				
δ-KY_3F_{10}	8.3% Eu^{3+} (M=5)	8.3% Eu^{3+} (M=7)	16.7% Eu^{3+} (M=7)	S10	Assignation
228.3	218.4-230.4 (10)	218.5-230.2 (10)	227.5-232.7 (3)	215	Bending F-Y-F
255.2	254.1-254.3 (2)	254.1-254.2 (2)	254.2 (1)	241	Bending F-Y-K
288.3	286.5-289.7 (3)	286.3-289.7 (3)	285.0-287.4 (2)	295	Bending F-Y-F
324.4	318.8-324.6 (3)	318.9-324.7 (3)	318.3-330.3 (3)	-	Bending F-Y-K
414.3	410.9-422.5 (4)	411.1-422.7 (6)	406.2-423.8 (4)	395	Stretching F-Y

Figure S1 shows the XRD patterns of samples doped with 50 and 100 mol% Eu^{3+} (S-50 and S-100). outlined in the main text, S-50 contains a mixture of different crystal phases: α-KY_3F_{10}, orthorhombic YF_3, hexagonal EuF_3, and orthorhombic EuF_3. On the other hand, sample S-100 also presents a mixture of hexagonal and orthorhombic EuF_3. This result highlights that it has not been possible to obtain the fully substituted KEu_3F_{10} compound, thus revealing the existence of a solubility limit of the dopant, at least, following the experimental procedure described in the present work.

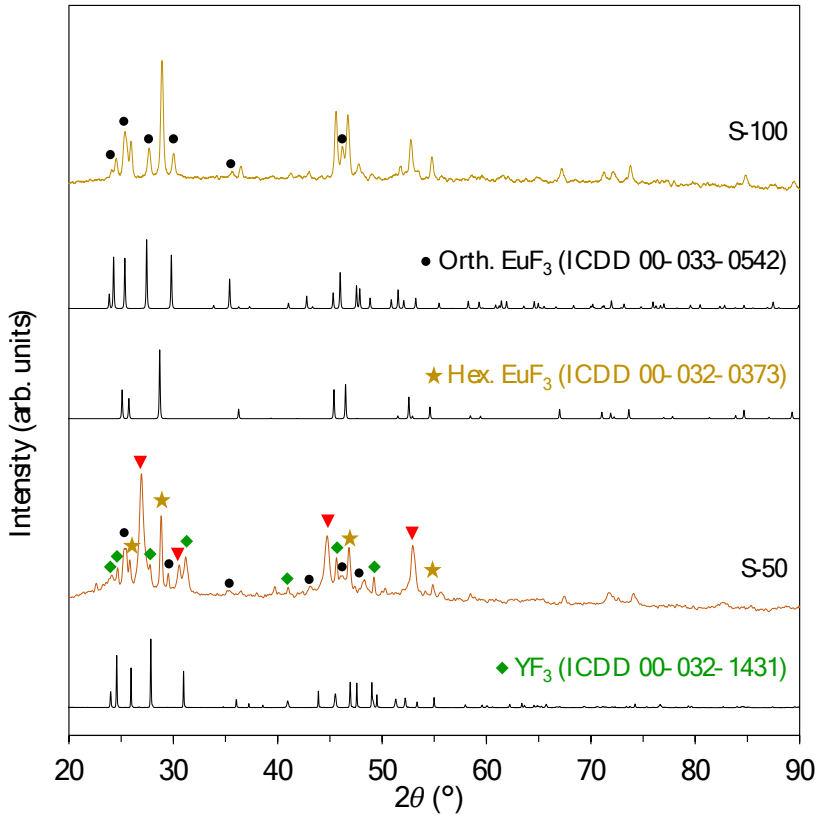

Figure S1. XRD patterns of samples doped with 50 and 100 mol% Eu^{3+} (S-50 and S-100). The peaks indicated with red triangles are associated to α-KY_3F_{10}, green diamonds refer to the presence of orthorhombic YF_3, ochre stars are associated to hexagonal EuF_3, while black dots indicate the peaks ascribed to orthorhombic EuF_3.

2. Computational methods

First principles calculations within the periodic DFT framework, with PBE0 [1] functional, were performed with the CRYSTAL17 [2] program to characterize the KY_3F_{10} and Eu^{3+} -doped KY_3F_{10}. 7-311G basis set[3] was used to describe F atoms and pseudopotentials were used to describe K [4], Y [5] and Eu [6] atoms. Regarding the density matrix diagonalization, the reciprocal space net was described by a shrinking factor of 4, corresponding to 36 k-points generated according to the Monkhorst−Pack scheme. The accuracy of the evaluation of the Coulomb and exchange series was controlled by five thresholds, whose adopted values were 10^{-8}, 10^{-8}, 10^{-8}, 10^{-8}, and 10^{-16}. A unit cell containing 56 atoms was used to study the δ-KY_3F_{10} and a supercell corresponding to 2 × 1 × 1 primitive cell (also with 56 atoms) was used to simulate the α-KY_3F_{10} system. Systems with a percentage of 8.3 and 16.7% of Eu^{3+} doping with respect to the Y^{3+} were simulated. The Raman vibrational modes and their corresponding frequencies were calculated from the unit cell and Eu^{3+} doped unit cell using numerical second derivatives of total energies as implemented in the CRYSTAL17 package.

To evaluate the stability of the Eu^{3+} doped models with respect to undoped system, we calculated the substitution energy (ΔE_{subs}) as follows:

$$\Delta E_{subs} = E(Eu^{3+}\text{- } KY_3F_{10}) - [E(KY_3F_{10}) + E_{Eu} - E_Y] \quad (1)$$

where $E(Eu^{3+}\text{- } KY_3F_{10})$ and $E(KY_3F_{10})$ are the total energies of the doped and undoped system, respectively, and E_{Eu} and E_Y are the energy per atom of Eu and Y metallic structures in the *Fm3m* space group. The calculated values are 0.12936 and 0.12920 Hartree (per unit formula) for the α and δ phases, respectively. These values indicate that the substitution process is associated with a comparable energetic cost in both structures, with a very small difference of approximately 1.6×10^{-4} Hartree (≈ 0.004 eV). This small

energy difference suggests that the Eu incorporation does not strongly favor one phase over the other from a purely energetic standpoint. Therefore, the concept of "chemical pressure" proposed in the manuscript can be interpreted as arising primarily from local structural distortions induced by the size and electronic differences between Eu^{3+} and Y^{3+}, rather than from a large energetic driving force for substitution.

In addition, configurations involving two Eu substitutions at different relative positions within the supercell were systematically examined. In this analysis, the first substitution was kept fixed, while all possible positions for the second substitution were explored. Our DFT calculations show that the total energy differences between these configurations are negligible. For the α phase, the differences appear only beyond the fifth decimal place in Hartree units, indicating that all configurations are energetically degenerate within the numerical accuracy of the method. For the δ phase, most configurations also exhibit negligible energy differences; however, three configurations show slightly higher energies, differing at the third decimal place in hartree units, as summarized in Table S3.

Table S3: Energy values (hartree) of configurations involving two Eu substitutions of α and δ-KY_3F_{10} phases.

Eu-subs	Energy δ phase	Energy α phase
5 e 6	-4.558087854678E+03	-4.558131650696E+03
5 e 7	-4.558087956081E+03	-4.558132383773E+03
5 e 8	-4.558087957588E+03	-4.558132621900E+03
5 e 9	-4.558087961357E+03	-4.558131386284E+03
5 e 10	-4.558087960000E+03	-4.558131254734E+03
5 e 11	-4.558087700806E+03	-4.558131386310E+03
5 e 12	-4.558087701571E+03	-4.558131252735E+03
5 e 13	-4.558088431006E+03	-4.558130767969E+03
5 e 14	-4.555442515668E+03	-4.558131814611E+03
5 e 15	-4.555444451477E+03	-4.558130768004E+03
5 e 16	-4.555442515891E+03	-4.558131814601E+03

Due to this near-degeneracy, the different dopant arrangements have effectively identical statistical weights in the α phase, and no preferential configuration can be identified. In the δ phase, although three configurations are slightly less stable, the energy differences remain small, and eight configurations are essentially equivalent. Consequently, the relative populations of these configurations are expected to be very similar, and no significant differences in local distortion or phase stability arise from the relative positioning of Eu dopants.

References

1. C. Adamo, V. Barone. *J. Chem. Phys*. 1999. **110** (13), 6158–6170.

2. R. Dovesi, A. Erba, R. Orlando, C. M. Zicovich-Wilson, B. Civalleri, L. Maschio, M. Rérat, S. Casassa, J. Baima, S. Salustro, & B. Kirtman. Wiley Interdisciplinary Reviews: Computational Molecular Science, 2018, **8**, 1–36.

3. R. Nada, C.R.A. Catlow, C. Pisani and R. Orlando, Modelling. Simul. Mater. Sci. Eng. 1993, **1**, 165-187.

4. M. Prencipe, Laurea Thesis 1990, (pages 91-92).

5. S. Gennard & F. Corà. 2000. https://www.crystal.unito.it/Basis_Sets/yttrium.html

6. Kh. E. El-Kelany, C. Ravoux, J. K. Desmarais, Y. Pan, J. S. Tse, R. Dovesi, A. Erba, *Phys. Rev. B* 2018, **97**, 245118.

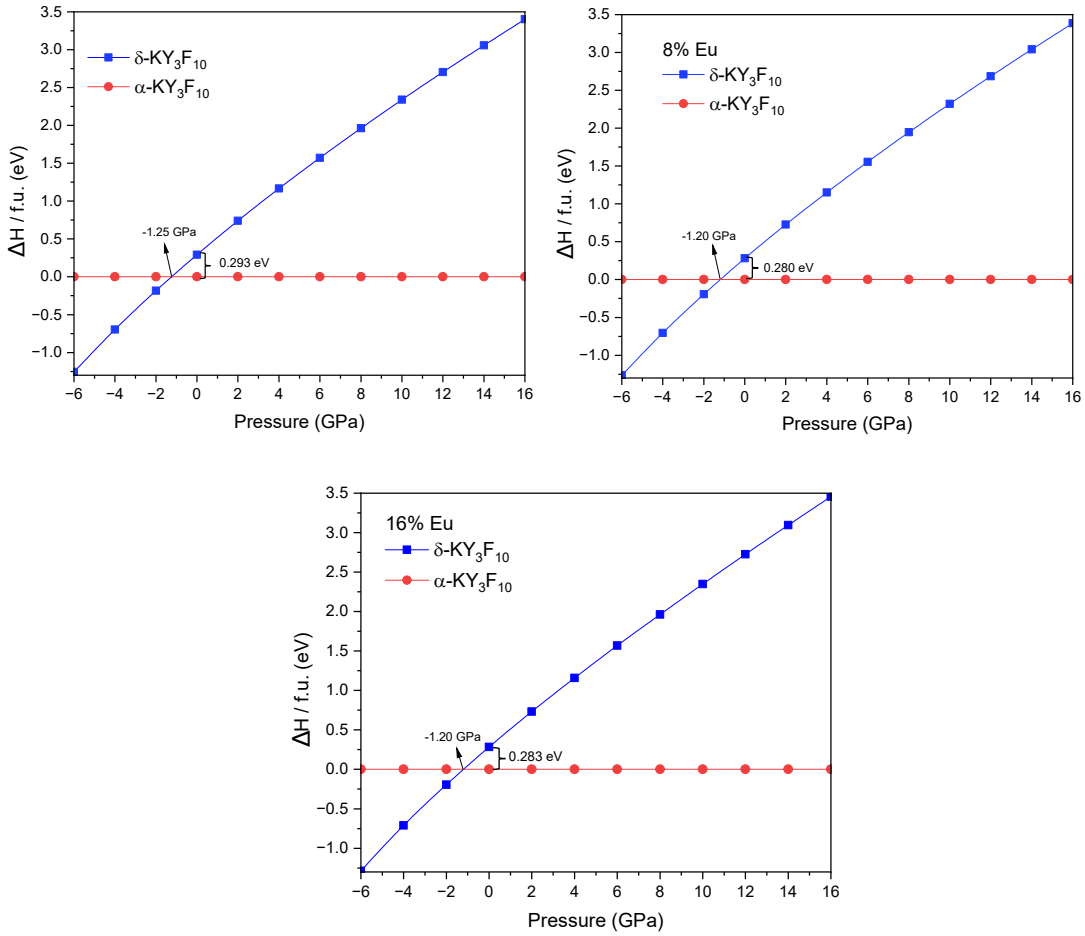

Figure S2. Enthalpy variation of α and δ–KY_3F_{10} polymorphs as a function of pressure for pure α to δ phase, at 8% and 16% of Eu^{3+} doping.

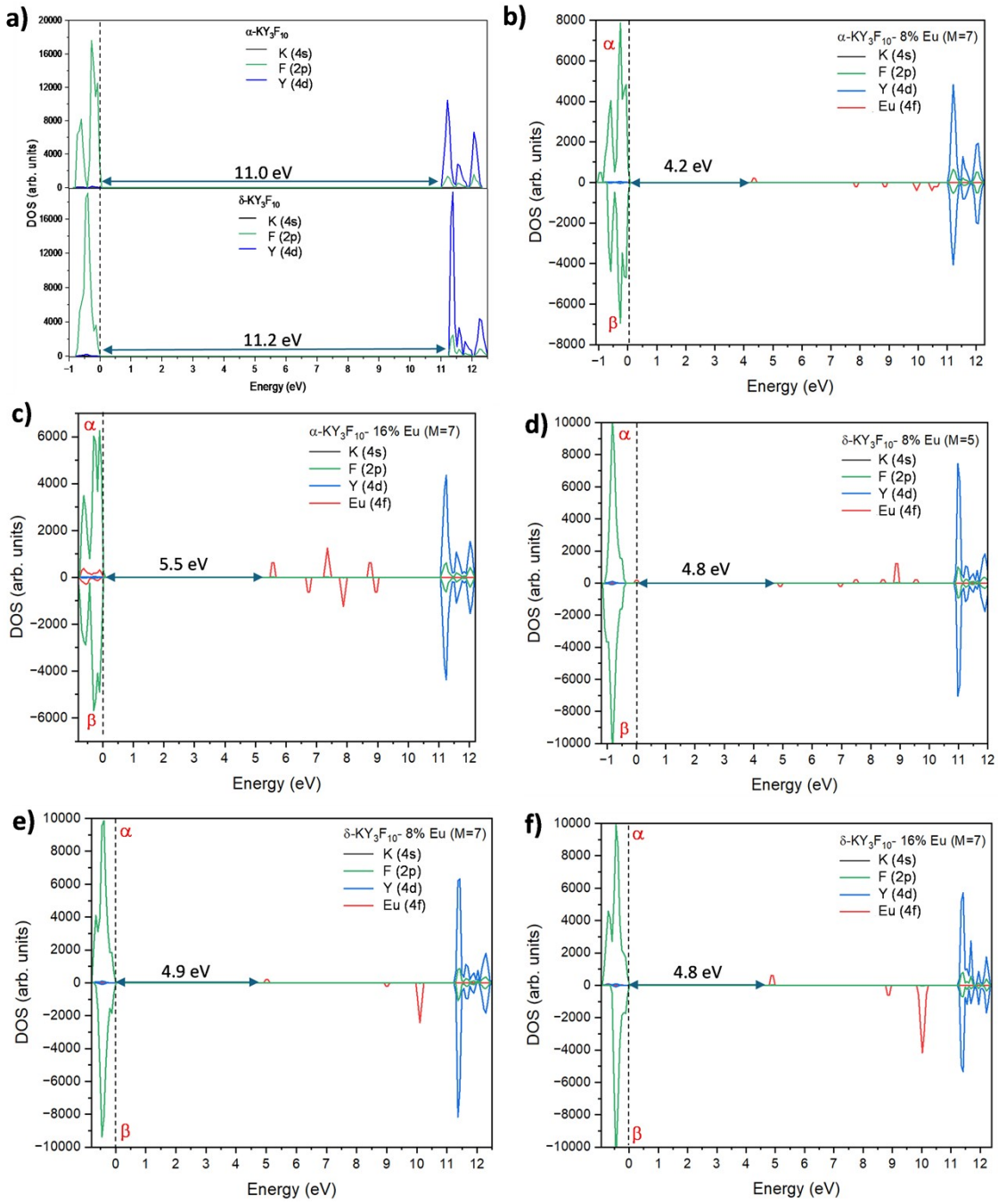

Figure S3. Projected DOS on atoms for (a) α and δ-KY_3F_{10} polymorphs, (b) α-phase at 8% Eu^{3+} (M=7), (c) α-phase at 16% Eu^{3+} (M=7), (d) δ–phase at 8% Eu^{3+} (M=5), (e) δ–phase at 8% Eu^{3+} (M=7) and (f) δ–phase at 16% Eu^{3+} (M=7). A vertical dashed line indicates the Fermi level. For clarity pourposes the position of 4f orbitals of Eu^{3+} at the band gap are highlighted in red color

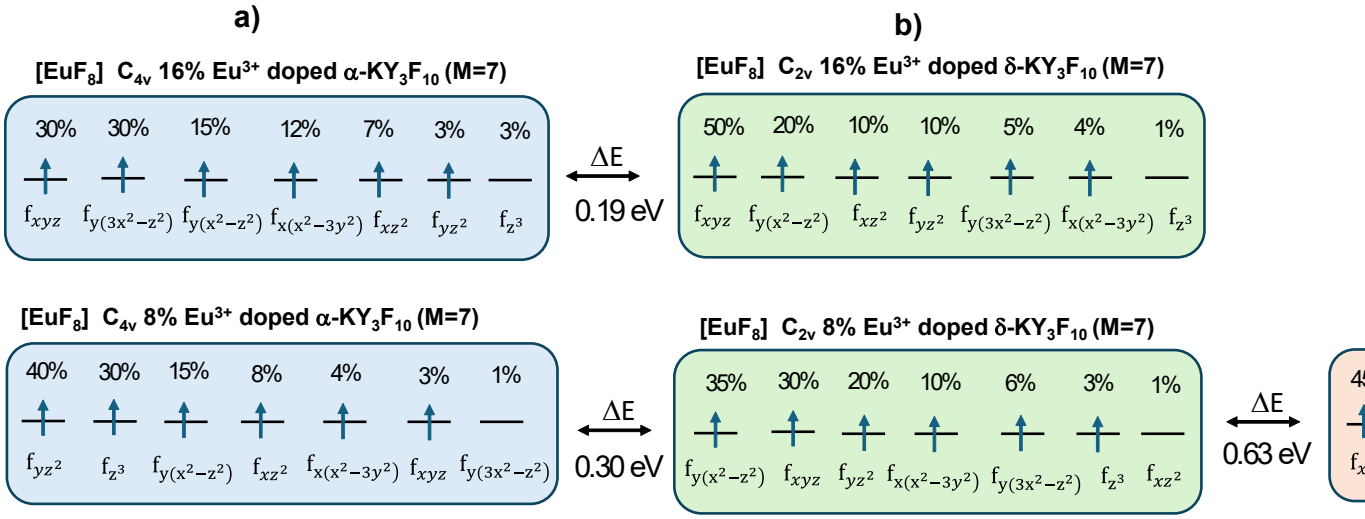

Figure S4. Electronic configurations for 4f orbitals of Eu^{3+}cation. a) 8% Eu^{3+} (M=7) and 16% Eu^{3+} (M=7) for α-phase, b) 8% Eu^{3+} (M=7) and 16% Eu^{3+} (M=7) and c) 8% Eu^{3+} (M=5) for δ−phase. The variation of energy in passing from one configuration to another is also included.